Philosophical Magazine Letters, 2014
Vol. 94, No. 6, 351–360, http://dx.doi.org/10.1080/09500839.2014.907509

Effect of geometrical constraint condition on the formation of nanoscale twins in the Ni-based metallic glass composite

M.H. Lee[a]*, B.S. Kim[a], D.H. Kim[b], R.T. Ott[c], F. Sansoz[d] and J. Eckert[e,f]

[a]*Rare Metals R&D Group, Korea Institute of Industrial Technology, Incheon 406-840, Korea;* [b]*Department of Metallurgical Engineering, Yonsei University, Seoul 120-749, Korea;* [c]*Division of Materials Sciences and Engineering, Ames Laboratory (USDOE), Ames, IA 50011, USA;* [d]*School of Engineering, The University of Vermont, Burlington, VT 05405, USA;* [e]*IFW Dresden, Institute for Complex Materials, P.O. Box 27 01 16, D-01171 Dresden, Germany;* [f]*TU Dresden, Institute for Materials Science, D-01062 Dresden, Germany*

(*Received 8 November 2013; accepted 16 March 2014*)

We investigated the effect of geometrically constrained stress–strain conditions on the formation of nanotwins in α-brass phase reinforced $Ni_{59}Zr_{20}Ti_{16}Si_2Sn_3$ metallic glass (MG) matrix deformed under macroscopic uniaxial compression. The specific geometrically constrained conditions in the samples lead to a deviation from a simple uniaxial state to a multi-axial stress state, for which nanocrystallization in the MG matrix together with nanoscale twinning of the brass reinforcement is observed in localized regions during plastic flow. The nanocrystals in the MG matrix and the appearance of the twinned structure in the reinforcements indicate that the strain energy is highly confined and the local stress reaches a very high level upon yielding. Both the effective distribution of reinforcements on the strain enhancement of composite and the effects of the complicated stress states on the development of nanotwins in the second-phase brass particles are discussed.

Keywords: twinning; metallic glasses; nanocrystallization; powder metallurgy; rapidly solidified materials

1. Introduction

When metallic materials are deformed under a compressive stress state at sub-ambient temperatures and/or high strain rates, grain refinement associated with a phase transformation such as recrystallization is often observed [1,2]. Growth or deformation twins are also commonly observed in nature, especially in face-centred cubic metals with relatively low stacking fault energies (i.e. Cu, Ni). Twins can also be formed by various approaches such as plastic deformation at sub-ambient temperatures and/or high strain rates, phase transformation, thermal treatment and other physical or chemical processes in a large variety of metals and alloys [3,4]. However, very fine-scale (nanoscale) twins are typically not observed experimentally under common deformation conditions for bulk metals [5].

Metallic glasses (MGs) have received a lot of attention because of their potential applications as high strength materials, however, under uniaxial compressive loading

*Corresponding author. Email: mhlee1@kitech.re.kr

the plastic flow is highly localized in shear bands, leading to catastrophic failure along one dominant maximum shear plane without global plasticity [6–9]. For this reason, metallic glass matrix composites (MGMCs) have been developed to provide enhanced plasticity under unconstrained loading conditions at temperatures below the glass transition temperature of the glass matrix. Specifically, MGMCs reinforced by particles [10], fibres [11], or *in-situ* formed ductile phase precipitates have been found to exhibit enhanced plasticity [12], not generally observed in monolithic bulk metallic glasses (BMGs). This deformation behaviour possibly stems from the formation of multiple shear bands initiated at the interface between the reinforcing phase and the MG matrix, and their confinement in MGMCs [13]. Moreover, an improvement in ductility has been demonstrated for MGMCs containing short brass fibres, synthesized by warm extrusion of powders, when loaded under uniaxial compression at room temperature [14]. The enhanced macroscopic plasticity is due to the formation of multiple shear bands initiated at the brass fibres/glass matrix interface.

Interestingly, deformation-induced crystallization of amorphous phase under hydrostatic pressure has been experimentally observed in Zr- and Al-based MGs [2,15] and numerically postulated in simple amorphous systems [16,17]. Furthermore, the formation of nanocrystals in Al-based amorphous ribbons plastically deformed by bending and Zr-based MG alloys subject to nanoindentation has been reported [1,18]. These experimental and computational results suggest that the nucleation of nanocrystals at shear bands during deformation may be related to geometrical constraint effects resulting from multi-axial stress conditions. However, in spite of previous observations, our understanding of the deformation-induced structural transformations in the reinforcement phase of BMG-matrix composites is still lacking.

In the present study, we investigated the effects of the complex stress-state that develops during loading on the formation of nanoscale twins in the reinforced particles and nanocrystallization in the matrix for a ductile brass phase reinforced $Ni_{59}Zr_{20}Ti_{16}$-Si_2Sn_3 metallic-glass-matrix composite deformed under quai-static uniaxial compression. We compare these results with regions of the glass matrix subject to a constrained geometry by the test platens, which lead to a local deviation from simple uniaxial compression to a multi-axial stress state, to evaluate the contrasting structural evolution that occurs under these different stress states.

2. Experiments

The Ni-based MG composite samples were prepared by hot extrusion of blended powders consisting of high-pressure gas atomized MG powder and α-brass ($Cu_{80}Zn_{20}$ wt.%) powder. The MG alloy powders produced by high-pressure gas atomization were sieved to −63 μm and combined with 40 vol.% brass (also <63 μm) in a Turbula blender. The powders were loaded into a copper can and sealed under vacuum for extrusion. Extrusion was performed by heating the billet to a temperature 845 K, which is above the glass transition temperature, but below the crystallization temperature of the MG (further details are given in Ref. [19]). Mechanical test specimens of brass reinforced Ni-based MG composite samples were cut and polished from extruded rods to produce rectangular specimens (2 mm width × 4 mm height). The uniaxial compression experiments, which were performed at room temperature, were done at a constant strain rate of $1 \times 10^{-4}\,s^{-1}$. Boron nitride (BN) was used as a lubricant between the sample and the

platens. For transmission electron microscopy (TEM) analysis, thin foils of the samples were prepared by ion milling using a Gatan Model 691 PIPS and TEM was performed with Jeol JEM 4010 and JEM 2000EX microscopes.

The Finite Element Analysis (FEA) performed with a two-dimensional (2D) finite element mesh was created with the FEA software OOF2 from an optical image of microstructure in the brass reinforced Ni-based MG composite (Figure 1a) [20], following the procedure described in Ref. [21]. The mesh was made of 2D plane-strain 3-noded and 4-noded linear elements. A general static analysis with a direct equation solver was carried with the FEA software ABAQUS. The mechanical behaviour of the Ni-based MG matrix was modelled as an elastic perfectly-plastic material with a constant flow stress σ_0. The brass particles were modelled with an elastic-plastic behaviour with isotropic hardening such as $\sigma_p = \sigma_0 + B(\varepsilon_p)^n$, where σ_p is the flow stress, ε_p is flow strain, B is strain hardening coefficient and n is strain hardening index. Table 1 lists the materials constants employed in the constitutive laws of our FEA simulations [22].

Uniaxial compression was simulated on the FEA mesh by fixing the nodes at the bottom boundary and displacing those at the top boundary along the loading direction. We also constrained the motion of the nodes on the left and right boundaries in order to simulate quasi-periodic boundary displacements. We impose a total compression

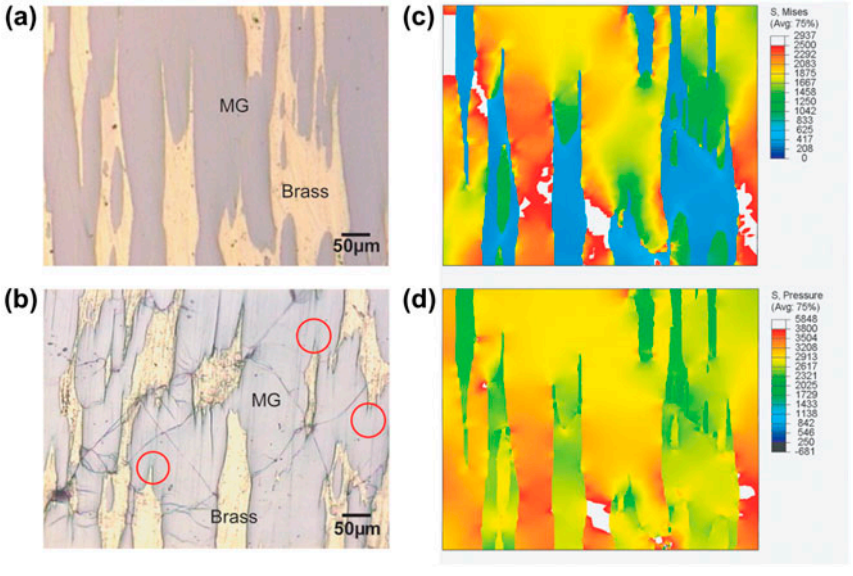

Figure 1. (colour online) (a) Optical microscope image taken from the longitudinal cross-section of the as-extruded brass reinforced Ni-based MG composite before the compression test; (b) Optical microscope image taken from the longitudinal cross-section of the brass reinforced Ni-based MG composite after the compression test. (marked circles show non-effective reinforcements); (c) Equivalent von Mises stress (i.e. shear stress) and (d) hydrostatic pressure predicted from FEA modelling of the composite structure corresponding to the micrograph in (a). The FEA shows effective local concentrations of shear stress and pressure under macroscopic uniaxial compression in regions where the second-phase particles are in close proximity to each other. The FEA model is deformed with 3.3% compression in the vertical direction.

Table 1. Materials constants for the constitutive laws used in FEA modelling.

Materials	Density (kg/m^3)	E (GPa)	v	σ_0 (MPa)	B (MPa)	n
Ni-based MG matrix	7930	123.1	0.356	2500	–	–
Brass particles	8520	90.0	0.318	247	505*	0.42*

*Ref. [22]

strain of 3.3%, which was found to result in a compression stress of ~1.6 GPa. The local shear stress and pressure were calculated from the equivalent von Mises stress and hydrostatic pressure determined at the integration points.

3. Results and discussion

Figure 1a and b show optical micrographs of the MG composites containing 40 vol.% brass reinforcements on the longitudinal (extruded direction) section before and after deformation, respectively. The room temperature flow stress of brass is 261 MPa, which is lower than that of the viscous flow stress (510 MPa) of the glass matrix during extrusion [19]. The relatively low strength of the brass and glass allows the mixed powder to be deformed readily during extrusion, as shown in Figure 1a. The role of the reinforcement for achieving plasticity and the progressive formation of shear bands in the glassy matrix during deformation was investigated by interrupted tests. Figure 1b shows the outer surface of the uniaxially compressed MG composite deformed to the maximum stress point (1.6 GPa) [19]. Upon yielding, a small number of shear bands initiates at the interface of the brass reinforcement and the matrix. During deformation, the load is effectively transferred from the glass matrix to the brass phase, leading to plastic deformation of the latter. From the FEA results shown in Figure 1c, we see that certain regions (the nearest effective distance between reinforcements) of the particle/matrix interface serve as local concentrations of shear stress, which would presumably lead to the initiation of shear bands. It is important to note that these stress concentrations correspond to regions where the particles are in relatively close proximity to each other. However, as noted by the circles in Figure 1b, the sharp points that are at the leading edges of the particles do not appear to lead to the initiation of shear bands. This is consistent with the FEA results, as presented in Figure 1c, which show that these regions do not have large localized shear stresses that would be favourable to shear band initiation. In addition to the shear stress being highly localized to regions where the particles are in close proximity, which allows the stress fields to "link up", the hydrostatic pressure is also localized to these regions, Figure 1d. As with the shear stress, the regions highlighted by the circles in Figure 1b even sharp corners of reinforcements show a significantly lower pressure compared to the more interconnected regions.

Figure 2a–d display bright field (BF) TEM images and corresponding selected area diffraction patterns (SADP) obtained before and after uniaxial compression of the Ni-based MG composite sample, respectively. The clear, featureless BF TEM image in Figure 2a shows the typical undeformed amorphous nature of the Ni-based MG matrix. A clear boundary without any visible reaction between the amorphous matrix and the brass phase is shown in Figure 2a. The SADP obtained from the brass phase marked in Figure 2b shows a typical [0 1 1] axis of the fcc structure.

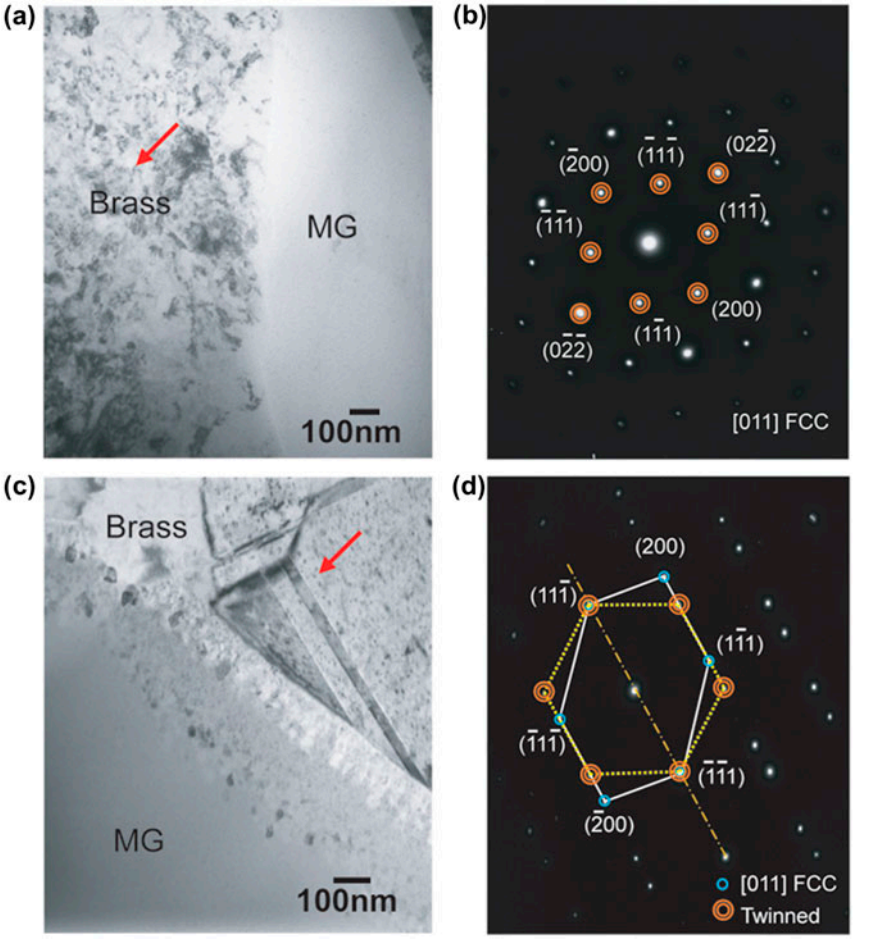

Figure 2. (colour online) Microstructural characterization related with phase transformation: (a) BF TEM image obtained from the as-extruded brass reinforced the Ni-based MG composite before deformation; (b) SADP obtained from the brass reinforcement (marked by the red arrow) of Ni-based MG composite before deformation showing a typical FCC crystallographic structure; (c) BF TEM image obtained from the brass reinforced Ni-based MG composite after deformation revealing nanoscale twins and adjacent nanocrystals; (d) SADP obtained from the brass reinforcement (marked by the red arrow) of the Ni-based MG composite after deformation showing a typical twinned structure.

Interestingly, the observation of nanotwins in the brass particles was always found to occur in the regions similar to those in Figure 1c and d, where the shear stress and pressure are highest.

In the case of the uniaxially deformed Ni-based MG composite sample, the BF field TEM image in Figure 2c shows nanocrystallites corresponded to Ni(Zr,Ti) and $Ni_{10}(Zr,Ti)_7$ phases with ~20 nm size in the MG matrix as well as twinning of the brass reinforcement. As with the nanotwinning, the experimentally observed nanocrsytallizaion is localized to areas where the FEA predicts the highest shear stresses and

pressures. Therefore, the stress state that promotes the nanotwinning in the second-phase particles also appears to promote crystallization in the glass matrix. While the predicted pressures do not approach the values predicted for indentation experiments, the correlation between nanocrystallization in the glass matrix and the concentration of shear stress and pressure might be similar to the observation of deformation induced crystallization under very high pressure generated by a diamond indenter [18].

The stress state of the specimen and the stress field at the specimen under compressive loading are depicted schematically in Figure 3a. The nominal locations of the schematic illustration represented where the TEM samples were obtained from the brass reinforced Ni-based MG composite, marked as regions A and B in Figure 3a, respectively. The Mohr–Coulomb yield criterion including the effect of compressive hydrostatic pressure (p) or the stress normal to the plane of shear yielding (σ_n) on plastic deformation is defined by $p = \sigma_m = -(\sigma_1 + \sigma_2 + \sigma_3)/3$, $\bar{\sigma} = 2\sqrt{(\sigma_1 - \sigma_2)^2 + (\sigma_2 - \sigma_3)^2 + (\sigma_3 - \sigma_1)^2}/\sqrt{2}$ [23]. The equivalent stress $\bar{\sigma}$ is given as a function of the stress triaxiality (χ) at yield. The level of stress triaxiality is defined as $\chi = p/\bar{\sigma} = \sigma_m/\bar{\sigma}$ where σ_m is the mean stress, and p is the hydrostatic pressure [23]. The relationship between the equivalent stress and the stress triaxiality is well matched by the Mohr–Coulomb criterion and the stress triaxiality is a linear function of the hydrostatic pressure [23–25]. The maximum stress levels corresponding to the initiation of shear bands for all combinations of tension and compression on shear are a function of the hydrostatic pressure [26]. The hydrostatic stress level is markedly elevated in the vicinity of a sharp corner of a whisker and can reach up to six times the overall yield strength [27]. For the microstructure of the Ni-based MG composite shown in Figure 1 (corresponded to region A in Figure 3a), the FEA predicts that localized regions are subject to a large hydrostatic pressure, even though the Ni-based MG composite specimen were macroscopically deformed under quasi-static uniaxial loading condition. This hydrostatic pressure arises from stronger, more compliant matrix that confines the particles during plastic deformation.

Along the brass particle-MG matrix interface, nanocrystallization of the amorphous matrix occurs within 100 nm of the boundary of the brass shown in Figure 2c. The structures of the nanocrystallites have been previously reported as correspond to Ni(Zr,Ti) and $Ni_{10}(Zr,Ti)_7$ compounds [28]. The SADP taken from the brass reinforcement marked in Figure 2d consists of two mirror-related [0 1 1] zones indicating {1 1 1} twinning of the fcc structure. As shown in Figure 3b, the nanocrystals in the MG matrix and the appearance of twinned structures in the brass particles indicate that upon yielding the highly confined strain energy saturates and the local stress reaches a very high level.

It is well known that nano-twinning can occur in low stacking fault energy (SFE) materials, such as brass (SFE_{brass} ~15 mJm^{-2}) for which the difficult nature of cross-slip can suppresses dislocation mobility [5]. Previous work has suggested that decreasing the twin spacing may enhance the work-hardening ability due to the twin boundaries acting as barriers to dislocation motion during plastic deformation, resulting in enhanced strength of fcc metals. [29] As shown in Figure 2c, the twin spacing observed in brass reinforcement has values from 30 to 55 nm ranges. It is reported that this twin spacing can be decreased down to 6 nm at the edge corner of a brass fibre surrounded by the matrix, which is expected to be represented a high level of hydrostatic pressure induced by multi-axial stresses [28].

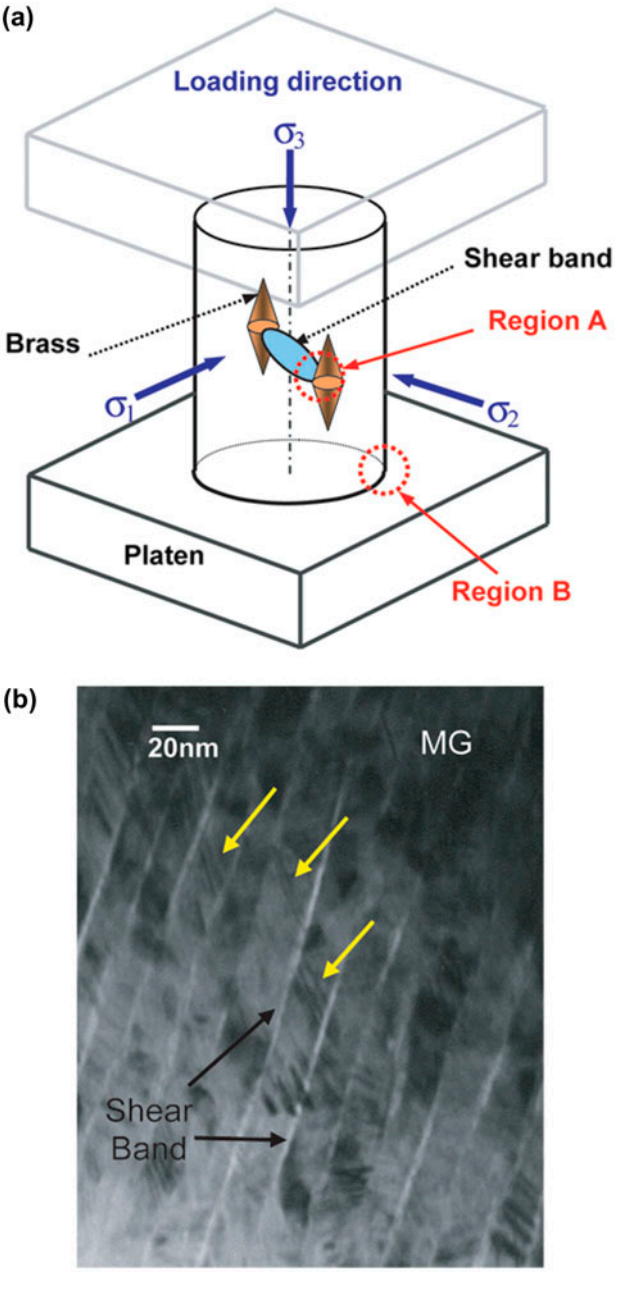

Figure 3. (colour online) (a) Schematic representation of the nominal locations where the TEM samples were obtained from the brass reinforced Ni-based MG composite; (c) BF TEM image obtained from the Ni-based monolithic BMG after deformation showing nanocrystallines (marked by the yellow arrows) generated around shear bands near the corner of the specimen (region B in Figure 3a).

The strengthening effect as a function of thickness (or lamella spacing) of nanoscale twins examined by Shen et al. via statistical TEM, was reported to follow the empirical Hall–Petch relation [29]. Furthermore, it has also been reported that the strain hardening coefficient of nanotwinned Cu increases linearly with decreasing twin boundary spacing [3]. Therefore, the brass reinforcement in the MG matrix acts both to diminish the work softening effect from shear banding in the MG matrix by blocking the shear bands propagation resulting in improved plasticity of the composite, and strengthening of the composite due to generation of nanotwins that impede dislocation motion in the second-phase brass particles.

The effects of the locally constrained geometry on the glass matrix can be further seen in the material adjacent to the upper and lower platens (corresponded to region B in Figure 3a), which his susceptible to non-uniform loading (stress state can deviate significantly from pure uniaxial compression). The evaluation of different regions of the glass matrix near the platens, but away from particle interfaces shows a propensity towards nanocrystallization in shear bands that form under multi-axial loading, as shown in Figure 3c. The friction stress induced by the planes at the lateral surface of the bottom part of the sample during compression is defined as $\sigma = \sigma_a[1 + \bar{m}/3\sqrt{3}\lambda_0 \times \exp(3\bar{\varepsilon}/2)]^{-1}$, where σ is the local von Mises equivalent flow stress of the material and $\bar{m}$ the friction parameter $(0 \leq \bar{m} \leq 1)$, $\bar{\varepsilon}$ is effective strain, μ is the Coulomb friction coefficient $(\mu = \bar{m}/2\sqrt{1-\bar{m}^2})$ at the compressed surface, σ_a is the apparent flow stress and $\lambda_0 = H_0/D_0$ is the initial aspect ratio of the specimen [23,30]. In the current study, σ_a is 2 GPa, λ_0 is 2, $\bar{\varepsilon}$ is 0.02 for the Ni-BMG and μ for the used boron nitride (BN) lubricant is 0.3 at room temperature. The calculated additional stresses from the friction-corrected effective flow stress for the uniaxial compression of a cylinder at region B is 550 MPa. Considering the temperature increase induced by heat generation due to friction, in case of very slow strain rate, it can be assumed that the sliding speed approaches a steady or quasi-static state. The temperature rise of the contact surface can be calculated by considering the heat generation equation at a single area of contact defined as $T(t) = 2h\sqrt{t}/\sqrt{\pi K \rho C_p}$ [31], where K is the thermal conductivity, ρ is the density, C_p is the specific heat and t is the time for which the heat is supplied and can be replaced by a/v. At the surface, the heat is supplied at a fixed rate with constant heat flux, and the average heat flux (h) at the contact area due to the frictional heating can be expressed as $h = \mu W v/\pi a^2$ [32], where μ is the coefficient of friction, a is the contact radius, v is the velocity and W is the load. In the current study, $\mu = 0.3$ for BN, $W = 1413$ N, $v = 3.3 \times 10^{-4}$ mm/s, $\rho = 7.9$ g/cm^3, $a = 0.5$ mm for the Ni-based BMG and $K = 7$ W/mK, $C_p = 500$ J/kgK for BMGs [33]. The calculated temperature rise by friction on the contact surface is only 1.48 K, because the accumulation of thermal energy by friction is more dependent on strain rate and contact area rather than the applied stress [34].

As shown in Figure 3b, the BF TEM image obtained from the lateral surface area of Ni-based monolithic BMG (region B in Figure 3a), which is close to the loading platens, shows shear bands resulting from the effect of stress triaxiality induced by friction. Moreover, shear bands and nanocrystallites can be seen simultaneously in the glass region B which is similar condition to the glass matrix adjacent to the brass particles, as shown in Figure 2c. This too is consistent with what we observed from the middle region of the sample. The major difference, however, is the route to dissipate strain energy. Nanocrystallization at amorphous matrix and nanotwinning at reinforcement are

more pervasive way in the strain concentrated region due to the overall stress triaxiality caused by the interfaces.

Several reports show that shear localization occurs by the formation of shear bands immediately upon the onset of plastic deformation [35,36]. The results of atomistic simulations of the deformation of MGs also show the influence of multi-axial stress states on yielding of MGs [24,25]. Other works have directly examined the role of multi-axial stress states on the plastic yield of MGs and one important consequence of shear localization in amorphous alloys is that the macroscopic yield criterion may exhibit a dependence not only on the maximum shear stress, but also on the hydrostatic pressure of the normal stress acting on the shear plane [37,38]. Deformation mechanisms based on the free volume or dilatation models [8,9], which involve the accumulation of free volume during localized shearing, would be expected to be pressure sensitive and to depend on the hydrostatic component of the applied stress [24,39].

Moreover, the formation of nanotwins might be expected to be observed outside the stress concentration regions, since the whole brass particles yield during the early stage of loading. However, it is possible that the interface structural incoherency at the brass particle-nanocrystalline MG boundary compared to that at the brass-amorphous interface introduces some free volume or microvoids at the boundary that would locally emit twinning partial dislocations in the brass particles.

4. Conclusions

In conclusion, during simple uniaxial compressive testing, the BMG matrix material adjacent to the edge corner of reinforcement is susceptible to non-uniaixal loading in which the effective stress state can deviate significantly from pure uniaxial loading. Moreover, there is effective distribution of reinforcements to support mechanical enhancement of composite material. Evaluation of different regions from the compressed Ni-based MG composite samples illustrates this geometrical constraint effect and the corresponding propensity towards nanocrystallization in the matrix and nanotwin formation in the brass reinforcement. The results highlight the complicated deformation behaviour of these metallic-glass-matrix composites under simple uniaxial compression. These new results can be used for the design and development of advanced MG composites which have an optimized configuration of reinforcements with superior mechanical properties.

Funding

This work was supported by the US Department of Energy under Contract No. DE-AC02-07CH11358 through the Cooperative Research and Development Agreement (AL-C-2012-04) between Ames Laboratory and KITECH. Work by RTO was supported by Office of Science, Basic Energy Sciences, Materials Sciences and Engineering Division under Contract No. DE-AC02-07CH11358, and FS thanks support from the National Science Foundation CAREER program (grant no. DMR-0747658). This work also supported by the Global Research Laboratory Program of the Korean Ministry of Education, Science and Technology.

References

[1] W.H. Jiang, F.E. Pinkerton and M. Atzmon, J. Appl. Phys. 93 (2003) p.9287.
[2] F. Ye and K. Lu, Acta Mater. 47 (1999) p.2449.
[3] L. Lu, X. Chen and K. Lu, Science 323 (2009) p.607.
[4] M. Chen, E. Ma, K.J. Heker, H. Sheng, Y. Wang and X. Cheng, Science 300 (2003) p.1275.
[5] J. Cai, S. Shekhar, J. Wang and M. Ravi Shankar, Scr. Mater. 60 (2009) p.599.
[6] A.L. Greer, Science 267 (1995) p.1947.
[7] C.T. Liu, L. Heatherly, J.A. Horton, D.S. Easton, C.A. Carmichael, J.L. Wright, J.L. Schneibel, M.H. Yoo, C.H. Chen and A. Inoue, Metall. Mater. Trans. A 29 (1998) p.1811.
[8] F. Spaepen, Acta Metall. 25 (1977) p.407.
[9] A.S. Agron, Acta Metall. 27 (1979) p.47.
[10] H. Choi-Yim, R. Busch, U. Köster and W.L. Johnson, Acta Mater. 47 (1999) p.2455.
[11] C.P. Kim, R. Busch, A. Masuhr, H. Choi-Yim and W.L. Johnson, Appl. Phys. Lett. 79 (2001) p.1456.
[12] C. Fan, R.T. Ott and T.C. Hufnagel, Appl. Phys. Lett. 81 (2002) p.1020.
[13] C.C. Hays, C.P. Kim and W.L. Johnson, Phys. Rev. Lett. 84 (2000) p.2901.
[14] D.H. Bae, M.H. Lee, D.H. Kim and D.J. Sordelet, Appl. Phys. Lett. 83 (2003) p.2312.
[15] D. He, Q. Zhao, W.H. Wang, R.Z. Che, J. Liu, X.J. Luo and W.K. Wang, J. Non-Cryst. Solids 297 (2002) p.84.
[16] B.J. Lee, J.C. Lee, Y.C. Kim and S.H. Lee, Met. Mater. Int. 10 (2004) p.467.
[17] N. Boucharat, R. Hebert, H. Rösner, R. Valiev and G. Wilde, Scr. Mater. 53 (2005) p.823.
[18] J.-J. Kim, Y. Choi, S. Suresh and A.S. Argon, Science 295 (2002) p.654.
[19] M.H. Lee, D.H. Bae, D.H. Kim and D.J. Sordelet, J. Mater. Res. 18 (2003) p.2101.
[20] S. Langer, R. Edwin Garcia and A. Reid (2012), OOF2. Available at http://nanohub.org/resources/oof2 (doi: 10.4231/D37W67515).
[21] R.T. Ott, F. Sansoz, J.F. Molinari, J. Almer, K.T. Ramesh and T.C. Hufnagel, Acta Mater. 53 (2005) p.1883.
[22] X. Jin and Y. Altintas, J. Mater. Process. Technol. 211 (2011) p.339.
[23] Y. Bao and T. Wierzbicki, Eng. Fract. Mech. 72 (2005) p.1049.
[24] A.C. Lund and C.A. Schuh, Acta Mater. 51 (2003) p.5399.
[25] P. Lowhaphandu, S.L. Montgomery and J.J. Lewandowski, Scr. Mater. 41 (1999) p.19.
[26] Y.M. Liang and K.M. Liechti, Int. J. Solids Struct. 33 (1996) p.1479.
[27] T. Christman, A. Needleman and S. Suresh, Acta Metall. 37 (1989) p.3029.
[28] M.H. Lee, D.H. Bae, D.H. Kim, W.T. Kim, D.J. Sordelet, K.B. Kim and J. Eckert, Scr. Mater. 58 (2008) p.651.
[29] Y.F. Shen, L. Lu, Q.H. Lu, Z.H. Jin and K. Lu, Scr. Mater. 52 (2005) p.989.
[30] C. Chovet, Ch Desrayaud and F. Montheillet, Int. J. Mech. Sci. 44 (2002) p.343.
[31] J.F. Archard, Wear 2 (1959) p.438.
[32] J.C. Jaeger, Proc. R. Soc. N.S.W. 66 (1942) p.203.
[33] U. Harms, T.D. Shen and R.B. Schwarz, Scr. Mater. 47 (2002) p.411.
[34] H.A. Abdel-Aal, Tribol. Int. 35 (2002) p.757.
[35] Z.F. Zhang, G. He, J. Eckert and L. Schultz, Phys. Rev. Lett. 91 (2003) p.045505.
[36] R.D. Conner, W.L. Johnson, N.E. Paton and W.D. Nix, J. Appl. Phys. 94 (2003) p.904.
[37] P.E. Donovan, Acta Metall. 37 (1989) p.445.
[38] J.J. Lewandowski and P. Lowhaphandu, Philos. Mag. A 82 (2002) p.3427.
[39] R. Vaidyanathan, M. Dao, G. Ravichandran and S. Suresh, Acta Mater. 49 (2001) p.3781.